Springer

KSME

Journal of Mechanical Science and Technology 24 (11) (2010) 2297~2305
www.springerlink.com/content/1738-494x
DOI 10.1007/s12206-010-0801-x

A study on the efficiency improvement of a passive oil damper using an MR accumulator †

Young-Won Yun[1], Seong-Min Lee[2] and Myeoung-Kwan Park[1,*]

[1]*School of Mechanical Engineering, Pusan National University, RIMT, Jangjeon-dong, Geumjeong-gu, Busan, 609-735, Korea*
[2]*School of Mechanical Engineering, Pusan National University, Jangjeon-dong, Geumjeong-gu, Busan, 609-735, Korea*

(Manuscript Received March 11, 2009; Revised January 12, 2010; Accepted July 15, 2010)

Abstract

This study describes the development, modeling, and testing of a hybrid damper for semi-active suspension. The goal of this study is to improve the performance of conventional passive oil dampers using a magneto-rheological (MR) accumulator that consists of a gas accumulator and an MR device. The level of damping is continuously variable by means of control of the applied current in an MR device that is fitted to a floating piston that separates the gas and oil chamber. A small MR device is used to resist the movement of the floating piston. At first, a mathematical model that describes all flows within the damper is formulated and developed in Matlab/Simulink. The MR device is also devised. A mathematical model is adopted to characterize the performance of the device. The formulas derived for the different components of the damper force are combined into a full damper model. Then, the applicability of the MR device to a conventional passive oil damper is tested in a manufactured test environment and evaluated in terms of the damping force vs. the piston velocity. From the results, it is possible to ascertain the MF device's capability to work as a damper that can supply a variable damping force. Moreover, this research affords a lot of new information about the applicability of MR devices and improvement of the damping force.

Keywords: Magneto-rheological fluids; Oil damper; Floating piston; Accumulator

1. Introduction

Dampers are one of the most important components in the motion of a vehicle in the interest of good handling and riding comfort. Much progress has been made in improving and optimizing vehicle damper design and technology that enable the improvement of overall vehicle performance, such as vehicle safety and road damage minimization, as well as good riding comfort and handling. Passive suspension systems always represent a compromise between riding comfort and handling, since stiffness is required for good handling, while a more compliant suspension is needed for good riding comfort. The force elements in these systems are not adjustable and cannot be controlled. Active suspensions, which require an external power source such as a hydraulic pump, can improve the performance of the suspension system over a wide range of frequency, but their energy consumption is considerably higher. Semi-active suspensions were proposed in the early 1970s [1]; they were receiving more attention than active suspension systems because of their low cost, low power requirement, and competitive performance in relation to active systems. Also, semi-active systems are safer than active suspension systems. When the control device of a semi-active system fails, the system still act as a passive damper, whereas if the failure of an active system occurs, an undesirable force can pull the tire away from the road, causing problems in vehicle handling and safety. Compared with passive and active suspension systems, there are advantages for developing semi-active systems. They provide comfort without compromising handling and stability and are simple, economical, and safe [2]. Although numerous so-called semi-active systems have been conceptualized, the basic concept has not changed much in the last few decades. Initially, the regulation of the damping force in semi-active systems was achieved by adjusting the area of the flow orifice in conventional oil dampers. These types of semi-active systems used mechanical valves driven by a solenoid or stepper motor to regulate the damper force in an oil-filled damper [3]. However, time delays and valve dynamics have been found to significantly affect the damper performance. In recent years, semi-active dampers using a functional fluid, such as magneto-rheological or electro-rheological (ER) fluids, have been widely studied to control the damping force of dampers by replacing the mechanical valves that commonly are used in adjustable dampers [4, 5]. The performance of an

† This paper was recommended for publication in revised form by Associate Editor Eung-Soo Shin

* Corresponding author. Tel.: +82 51 510 3089, Fax: +82 51 514 0685
E-mail address: mkpark1@pusan.ac.kr

MR or ER damper has been evaluated for various applications, especially to attenuate undesirable vibration. Although mechanical and rheological control dampers have been extensively researched and developed, a damper is also needed to reduce cost and weight.

This paper proposes a hybrid damper that combines a conventional passive oil damper with an MR device to obtain the effect of various damping forces as well as reduce cost and weight. Normally, in passive dampers, the pressure difference between the compression and rebound chamber drives the flow and generates the damper force. When an additional force that can change the pressure difference is supplied, the pressure difference can be adjusted and controlled. In this study, an MR device is employed to supply an additional force and fitted to the floating piston in a gas chamber. The pressure in the gas chamber affects the pressure in the compression chamber and is a function of the displacement of the floating piston. In other words, the pressure difference in the damper is regulated by means of control of the displacement of the floating piston, resulting in a change in the damping level. Therefore, the level of damping is continuously variable through control of the magnitude of the applied magnetic field in the MR device that is fitted to a floating piston. The simple MR device is used only to provide a force that can restrict the movement of the floating piston; that is, the directions of movement of both the damper and floating pistons are the same.

This paper is organized as follows. The next section presents a description of the operating method and components of the hybrid damper used. The third section discusses a mathematical model that well describes all flows within the damper. Also, this section presents a mathematical model that is adopted to characterize the performance of an MR device. The fourth section discusses the simulation and experimental results of the proposed hybrid damper. The last section summarizes the results of this work and provides recommendations for future work.

2. Concept and operating methods of hybrid dampers

A functional representation and configuration of a hybrid damper, with schematics of the components that are necessary for its operation, are shown in Figs. 1 and 2, respectively. The hybrid damper consists of a conventional passive oil damper with an external tank-type reservoir and an MR accumulator. The MR accumulator is also comprised of a gas accumulator and a device of the MR-damper type. Inside of the MR accumulator, one shaft of the MR device is fitted to a floating piston. This damper is partitioned into four pressure chambers: the compression chamber, rebound chamber, gas chamber, and MR fluid chamber. In the gas chamber, a compressible gas, such as nitrogen, is used as the springing medium; it is separated from the compression chamber by the floating piston. In both the compression and rebound chambers, a hydraulic fluid is used to convert pressure to force. The MR chamber

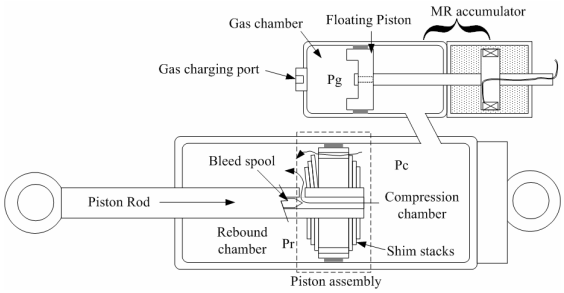

Fig. 1. The schematic configuration of the hybrid damper in this study.

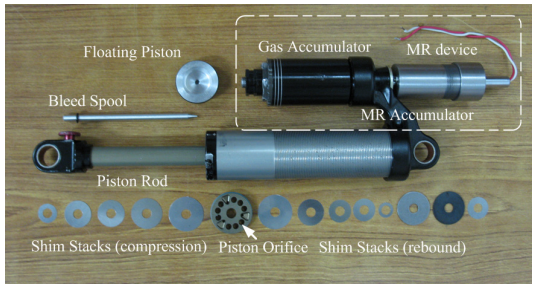

Fig. 2. Configuration of a hybrid damper.

is completely filled with an MR fluid. The MR device has a fixed-size orifice with the ability to apply a magnetic field, using an electromagnet, to the orifice volume.

This magnetic field results in a change in the viscosity of the MR fluid, causing a pressure differential for the flow of fluid in the orifice volume. The pressure differential is directly proportional to the force that is required to move the rod of the MR device. As such, the characteristics of the damping force in the MR device is a function of the electrical current flowing into the electromagnet. This relationship allows the damping force of the MR device to be easily controlled in real time. The accumulator is a pressurized volume of gas that is physically separated from the hydraulic fluid by a floating piston. The accumulator serves two purposes. The first is to provide a volume for the hydraulic fluid to occupy when the piston rod is inserted into the cylindrical housing. The second is to provide a pressure offset so that the pressure in the low-pressure side of the piston assembly does not induce cavitation in the hydraulic fluid by reducing the pressure below the vapor pressure of the hydraulic fluid.

During the compression stroke, the hydraulic fluid in the cylindrical housing flows from the compression chamber into the rebound chamber. For the rebound stroke, the pressure definitions become the opposite and the flow reverses. These flows passing through the piston assembly are related to the pressure differences in the pressure chambers. These pressure differences drive the flow from the compression chamber to the rebound chamber and generate the damping force. At low-speed conditions, the damping force is caused by the resistance of fluid that passes through some orifices. At high-velocity conditions, the fluid pressure is high enough to deform the shim stacks and the fluid can also pass through the

space between the shims and piston orifices. Since the fluid is effectively incompressible, as the piston rod enters the rebound chamber, the sum of the volumes of the fluid and the rod in the rebound and compression chambers must increase. To accommodate the increased volume, the floating piston compresses the nitrogen gas in the gas chamber to decrease the gas volume by an amount equal to the volume of the inserted rod. In reality, the pressure in the compression chamber is a function of the piston acceleration, gas-chamber pressure, and piston displacement. Additionally, the effect of the acceleration is much smaller than the pressure in the gas chamber, which effectively shows that the gas pressure, which is a function of the floating-piston displacement, affects the pressure in the compression chamber. Considering an additional force that can adjust the movement of the floating piston, the pressure in the compression chamber will be regulated. Consequently, the force that is generated by the MR device that is used to restrict the movement of the floating piston plays an important part in causing the pressure differences; hence, the damping force that is augmented by an additional force produces a pressure drop across the damper piston assembly. The augmentation will be accomplished by the magnitude of the applied magnetic field in the MR device.

3. Damper modeling

Several papers deal with modeling methods of automotive dampers, which are commonly referred to as shock absorbers [6, 7, 8]. One of the most significant contributions is due to Reybrouck, who presented a shock absorber model that has twenty one parameters that correspond to various physical properties and tuning possibilities of a standard automotive damper [7]. These parameters can be used to specify damping behaviors in a precise and practical manner. This is the main difference between this model and other published damper models. Flow restriction forces were found using empirical relationships that included leak restrictions, port restrictions, and spring stiffness correction factors. Once individual internal forces were found, another empirical relationship was used to calculate the total damping. Pressure drops across the specific flow restrictions could also be found. Although numerous correction factors for implementation of this model are necessary, this model shows excellent correlation with experimental data in the range of low stroking frequency.

In this paper, the Reybrouk model is used as the basis for the model of a conventional oil damper. During the compression stroke, the fluid in the compression chamber flows into the rebound chamber. The rebound stroke is the reverse process in which the rod is withdrawn from the fluid filled chamber, causing flow from the rebound to the compression chamber. The total flow during the stroke is comprised of flow through two flow paths. These flows are related to the pressure differences in the pressure chamber. Two flow restrictors are present in each flow path to restrict the flow. The first restrictor restricts the flow of fluid through the bleed port. The second is a shim restrictor that restricts the flow through the piston orifice. These restrictors contribute to the total damping force. Fig. 3 shows the arrangement of all the flow paths.

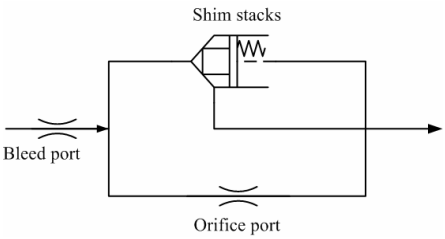

Fig. 3. The arrangement of the entire flow path in the piston assembly.

3.1 Restriction force of the bleed port

The bleed port dominates the low-speed damper because it is always open. The area of the port can be adjusted by modifying the geometry of the bleed spool or size of the bleed port. The damping force generated by the bleed port can be represented as follows [7]:

$$F_{bleed} = K_{bleed} \nu^{0.25} \dot{x}_p^{\ 1.75} - K_{hys} \ddot{x}_p . \quad (1)$$

In Eq. (1), K_{bleed} is the bleed restriction parameter that governs the magnitude of force generated by the leak restriction, $\nu (= 26\text{e-}5 m^2/s)$ is the kinematic viscosity of oil, and $\dot{x}_p$ is the velocity of the damper piston. K_{hys} is the bleed hysteresis parameter for presenting the effect of hysteresis. Hysteresis was caused by not only oil compressibility but also the compressibility of gas bubbles that were transferred from both chambers. The term is added to or subtracted from the restriction force of the bleed port depending on the damper motion.

3.2 Restriction force of the piston orifice and shim stacks

After traveling through constant-bore holes in the piston, the flow passes through thin washer-like shims that deflect to allow flow. The increased velocity decreases the pressure in the rebound chamber and increases the flow rate. For the compression stroke, the shim located in the rebound chamber limits the flow of fluid depending on the velocity of the piston. With increased velocity, the deflection of the shim increases and the flow increases. The flow through the piston assembly, except the bleed port, must be broken up into two parts: flow through the piston orifice port and flow that contacts the shim stack and exits. This flow through the shim stack is referred to as flow through the valve. First, the restriction force of the piston orifice can be expressed as follows [7]:

$$F_{orifice} = K_{orifice} \nu^{0.25} \dot{x}_p^{\ 1.75} . \quad (2)$$

In Eq. (2), $K_{orifice}$ is the orifice restriction parameter that governs the magnitude of the force that is generated by the

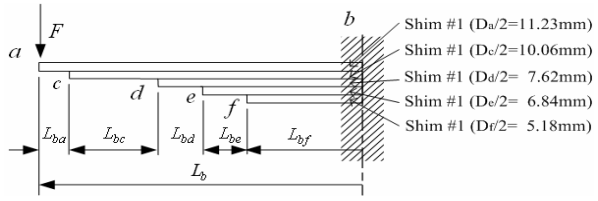

Fig. 4. The shim-stack model.

orifice restriction. The flow leaving the piston orifice contacts the large shim and turns by 90°. Then, the second pressure drop occurs across the shim stacks after the flow exits the piston orifice.

The shim stacks are a series of thin circular steel discs stacked according to diameter. By considering the stiffness, K_{spring}, of the shims, the deflection, δ, of the shim stack can be approximately expressed by:

$$F_{shim} = F_{preload} + K_{spring}\delta \tag{3}$$

where F_{shim} is the force due to the pressure on the surface of the largest shim and $F_{preload}$ is the pre-load force. The deflection of the shim stacks is an unknown parameter, and can be determined from the method of superposition [9]. Fig. 4 shows a cantilever beam to illustrate this method for shim stacks.

The shim stacks used in our study are constructed of five kinds of shim, which have different diameters. Provided that, for example, the beam is held rigidly at point C, it neither deflects nor rotates at that point. Then, the defection of the end, δ_a, can be calculated and expressed as follows:

$$\delta_a = \frac{FL_{ba}{}^3}{3EI}. \tag{4}$$

In addition, part CD of the beam also behaves like a cantilever and contributes to the deflection of the end. The deflection and angle of point C are:

$$\delta_c = \delta_c + \theta_c\left(L_{bc}\right) = \frac{7FL_{bc}{}^3}{6EI}. \tag{5}$$

In this manner, the calculation of the points of deflection of D, E, and F and summation yield:

$$\begin{aligned}\delta_t &= \delta_a + \delta_c + \delta_d + \delta_e + \delta_f \\ &= \left(\alpha_1 L_{ba} + \alpha_2 L_{bc} + \alpha_3 L_{bd} + \alpha_4 L_{be} + \alpha_5 L_{bf}\right)\frac{F}{EI}\end{aligned} \tag{6}$$

where $\alpha_i\,(i = 1 \sim 5)$ is constant values of the beam length. To find the stiffness, K_{spring}, of the shim stacks, the substitution of the moment of inertia, $I = bt^3/12$ (where b is the width and $t = 0.24mm$ is the thickness of shims), into Eq. (6) and division of the load by the deflection yield:

$$\begin{aligned}K_{spring} &= \frac{F}{\delta_t} \\ &= F/\left(\alpha_1 L_{ba} + \alpha_2 L_{bc} + \alpha_3 L_{bd} + \alpha_4 L_{be} + \alpha_5 L_{bf}\right)\frac{12F}{Ebt^3} \\ &= \chi t^3\end{aligned} \tag{7}$$

Eq. (7) shows that the effective stiffness is proportional to the cube of the thickness of the shim. χ is a constant value if all other input variables are changed.

3.3 Gas accumulator

In an oil damper with an accumulator, the gas chamber accounts for the increase in volume caused by the insertion of the rod. The relationship between the accumulator force and displacement was derived under the following assumptions [10].

(1) The seal friction between the floating piston and cylinder wall is neglected.
(2) The initial and final temperatures are the same.
(3) Nitrogen behaves as an ideal gas.
(4) Nitrogen undergoes a polytropic expansion and compression process with a polytropic exponent, $n = 1$.

Through the above assumptions, the pressure in the gas chamber can be expressed as:

$$P_g(x_f) = P_{go}\frac{A_{float}L}{A_{float}L - A_{rod}x_p} \tag{8}$$

where P_g is the gas pressure at any time and a function of the displacement of the floating piston. P_{go} is the initial precharged pressure, A_{float} (where, $d_f = 0.027m$) is the area of the floating piston, A_{rod} (where, $d_{rod} = 0.0128m$) is the area of the piston rod, and L $(= 0.026m)$ is the chamber length of the accumulator. By multiplying the pressure in the accumulator by the area of the floating piston, the force produced by the gas chamber is:

$$F_{gas}(x_f) = F_{go}\frac{1}{1 - (A_{rod}/A_{float})(x_p/L)}. \tag{9}$$

The displacement of the floating piston can be estimated by the damper piston. Assuming the fluid is incompressible, the value of x_f is to be established from x_p. To evaluate the reasonableness of this assumption, a test for investigating a relationship between both pistons is conducted by using a laser displacement sensor and its result is shown in Fig. 5. The discrepancy between the experimental results is because the fluid is compressible and contains a small amount of air entrained as bubbles, which can increase the compressibility and cause hysteresis in both high- and low-velocity regions. Although a slight discrepancy is found between the results, the above assumption is relatively reasonable and hence, an appropriate proportional gain is to be selected.

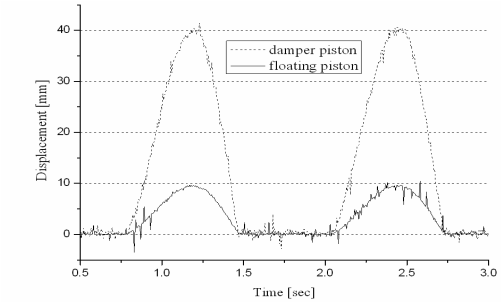

Fig. 5. The relationship between the damper and floating pistons.

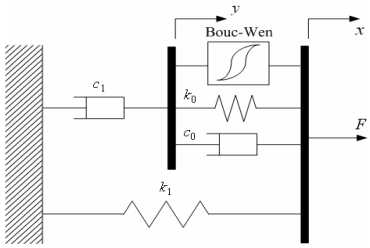

Fig. 6. Mechanical model of the MR device.

Table 1. Model parameters identified for MR device used in this paper.

Parameter	Value	Parameter	Value
c_{0a}	5.8 [Ns/m]	α_a	69.5 [Ns/m]
c_{0b}	21.6 [Ns/mV]	α_b	501 [Ns/mV]
k_0	20 [N/m]	γ	480 [m^{-2}]
c_{1a}	100.5 [Ns/m]	β	480 [m^{-2}]
c_{1b}	850.3 [Ns/mV]	A	301
k_1	5.0 [N/m]	n	2
x_0	0.02 [m]	η	190 [s^{-1}]

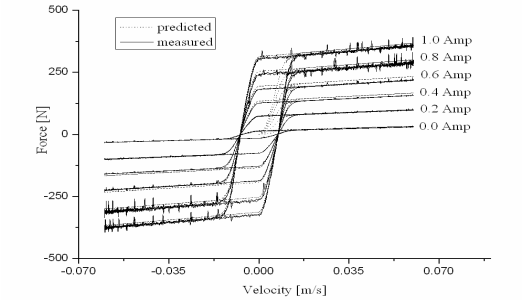

Fig. 7. Comparison between the predicted and measured data.

3.4 MR device

The MR device, which fitted in series to the side of the gas accumulator, comprises a bobbin and a flux return that form an annulus through which the MR fluid flows. The bobbin is wound with an insulated wire core. An input current that is applied through the coil around the bobbin creates a magnetic field in the gap between the bobbin and flux return. The magnetic field increases the yield stress of the MR fluid between the bobbin and flux return. By varying the yield stress, the device produces a damping force through the fluid flowing resistance in the gap by creating a plug flow. The mathematical model proposed by Spencer et al. is adopted in this study [11]. The hysteresis behavior in the MR device is described by the Bouc-Wen model. Fig. 6 shows a schematic of the model. In this model, the equations governing the force F_{mr} predicted by this model are:

$$F_{mr} = c_1\dot{y} + k_1(x - x_0),$$
$$\dot{y} = (1/c_0 + c_1)[\alpha z + c_0\dot{x} + k_0(x - y)] \quad (10)$$

where

$$\dot{z} = -\gamma|\dot{x} - \dot{y}||z|^{n-1} - \beta(\dot{x} - \dot{y})|z|^n + A(\dot{x} - \dot{y}),$$
$$\alpha = \alpha_a + \alpha_b u,$$
$$c_0 = c_{1a} + c_{1b}u,$$
$$c_1 = c_{1a} + c_{1b}u, \text{ and}$$
$$\dot{u} = -\eta(u - v).$$

Above, x is the displacement of the MR device, z is an evolutionary variable that accounts for the historical dependence of the response, and y is the internal pseudo-displacement of the MR device. In this model, c_0 and c_1 are the viscous damping force coefficients observed at large and low velocities, respectively; k_1 is the accumulator stiffness; k_0 is the gain to control the stiffness at large velocities; x_0 is the initial displacement of the spring; γ, β, and A are the hysteresis parameters for the yield element; α is the evolutionary coefficient; u is the output of a first-order filter; and v is the command voltage sent to the current driver. The values obtained for the above parameters can be determined by fitting the model to the data obtained from the experiments.

Through the optimization method in MATLAB and experimental results on the MR device, the coefficients of the model are determined and listed in Table 1.

Fig. 7 provides a comparison between the predicted and measured responses that are obtained for this device under a manufactured system, where the excitation frequency and magnitude of the input sinusoid wave are selected as 1 Hz and 20 mm, respectively. It is clearly observed that the proposed model can capture the properties of the MR device except at the region where the velocity is near zero.

3.5 Consolidated damping force

The summation of the forces caused by these pressure drops over the bleed port, piston orifice, and shim stacks yields a relationship for the total damping force. The sum of the forces can be computed as follows:

$$F_{damper} = F_{damping} + F_{gas} + F_{friction}\,\mathrm{sgn}(\dot{x}) + F_{mr} \quad (11)$$
$$F_{damping} = (P_c - P_r)(A_p - A_r) = F_{bleed} + F_{orifice} + F_{shim} \quad (12)$$

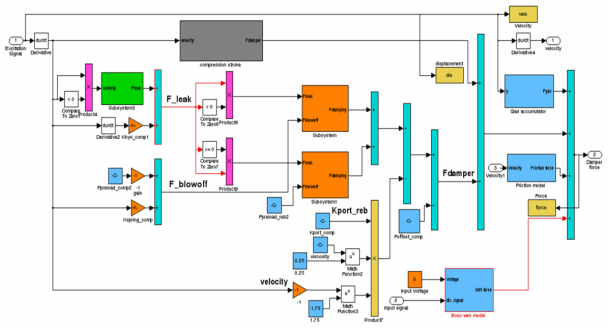

Fig. 8. Simulink block-diagram for the entire model.

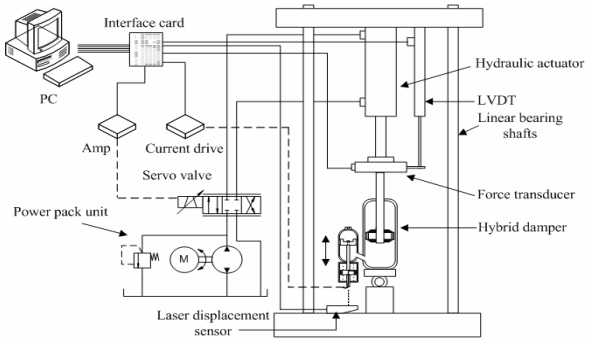

Fig. 9. Schematic of the equipment for the experimental test.

In the above equations, F_{damper} is the damper shift force and $F_{friction}$ is the frictional force between the piston seal and inner wall of the cylinder and between the rod and seal. All the simulations are performed using Matlab/Simulink and the Simulink block diagram model is constructed as shown in Fig. 8. The ODE45 (fourth-order Runge-Kutta) numerical integration algorithm is used for simulations and an error tolerance of $1e^{-5}$ is prescribed.

4. Comparison of the numerical and experimental results

Using the test equipment depicted in Fig. 9, preliminary tests were conducted to obtain experimental data on the damper-force characteristics. This equipment was manufactured to accomplish the research objectives and be capable of inputs ranging from signal frequency waveforms through to step and ramp inputs. To avoid any lateral loading on the actuator, a swivel jig was incorporated in the installation between the actuator and damper.

By adjusting the amplitude and frequency, a wide range of desired velocities can be achieved. The hardware includes a compatible personal computer (Pentium 1 GHz) that supplies the input signal to the hybrid damper and controls the servo valve though an MF 624 multifunction I/O card with the Real-Time Toolbox of Matlab/Simulink. The MR device is controlled by a current drive to supply the current.

The equipment is tabulated in Table 2. To obtain plots of the force vs. velocity, a load cell and LVDT are compatibly

Table 2. The list of equipment used.

No.	Name	Model name	Company
1	Servo valve	J076-103 J0345	Moog Co.
2	Servo valve amp	J121-001 J0547	Moog Co.
3	Load cell	MNT-500L	CAS Co.
4	LVDT	LTM 300S	GEFRAN
5	Laser displacement sensor	LB-1201	KEYENCE
6	Wonder box current device controller kit	RD-3002-03	LORD Co.
7	Multifunction I/O card with the Real-Time Toolbox	MF624	HUMUSOFT

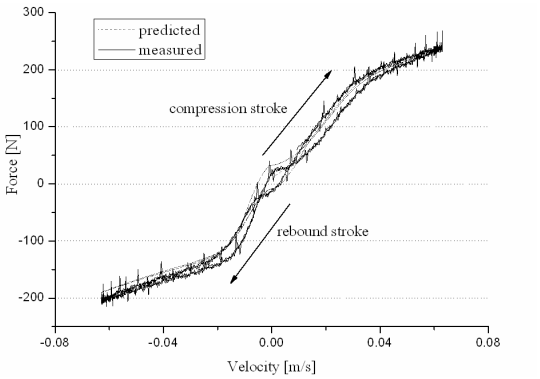

Fig. 10. Comparison between the predicted results and measured data for an oscillation frequency of 1.0 Hz with a 20 mm-displacement amplitude in the absence of an applied magnetic field.

equipped and the computer collects and records the measured data. The velocity and acceleration are obtained by differentiating a low-pass filtered displacement measurement. The computer code is programmed in the MATLAB environment. The method of testing the damper is to use a sine wave input and control the frequency. The damper was stroke about its endpoint for each test. All tests were accomplished at about $25^{\circ}C$. The damper was given time to cool between individual tests for avoiding heat-transfer effects between the gas chamber and surroundings. The pre-charging pressure in the gas chamber of each test was 0.5 MPa. The values from the measured data were used to identify the parameters of the simulation model. To achieve good results, it is necessary to accomplish several iterative processes. Note that compression results in positive velocities, while rebound results in negative velocities. This convection was followed throughout this work. In the first test, the bleed restriction parameter was identified by fitting a test curve at low velocity. Fig. 10 shows the measured damping-force characteristics at an excitation frequency of 1.0 Hz. In testing, a solid shim was placed over the valve orifices in the piston to block flow that passed through from the compression to the rebound chambers. Therefore, during the piston stroke, fluid only flowed through the bleed port. The values of K_{bleed} and K_{hys} were adjusted to obtain a correlation between the predicted and measured data. It is observed that

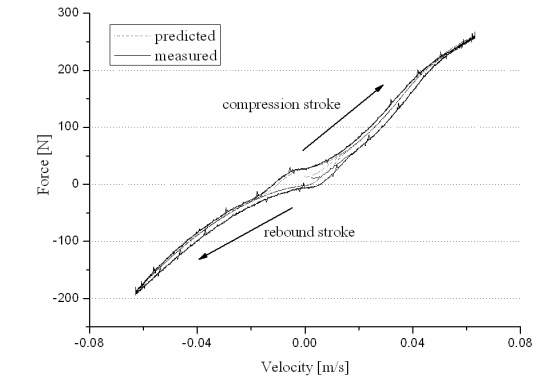

Fig. 11. Comparison between the predicted results and measured data for an oscillation frequency of 1.0 Hz with a 20 mm-displacement amplitude in the absence of an applied magnetic field.

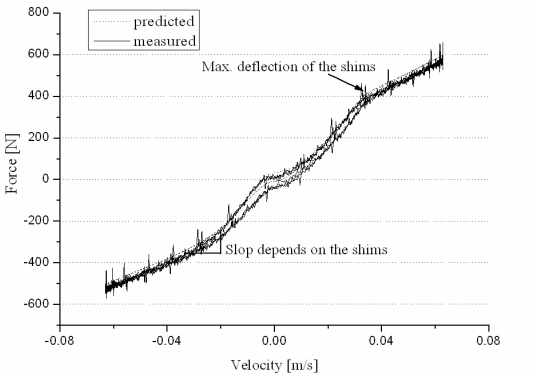

Fig. 12. Comparison between the predicted results and measured data for an oscillation frequency of 1.0 Hz with a 20 mm-displacement amplitude in the absence of an applied magnetic field.

the agreement between the predicted and measured results is good, but a slightly discrepancy is shown in Fig. 10. The small loop at zero velocity is due to both the flow resistance in the MR device and frictional force from the seal. It is also thought that the loop is caused by not only the pressure of the pre-charged gas chamber but also the small pressure difference in the transition from compression and rebound.

The second test was accomplished in the absence of shim stacks by closing the bleed port so that only fluid passed through the piston orifices. The used piston orifices contained nine straight orifices that had diameters of 4.1 mm (soft damping) and three that had diameters of 2.0 mm (hard damping). Fig. 11 displays the results for the piston orifices tested. From this result, the restriction parameter of piston orifices is identified by fitting. The agreement between the predicted results and measured data is reasonable. The total area of the piston orifices is larger than the bleed area. Hence, in low-velocity regions, the slope of the force caused by piston orifices is gentler than that caused by the bleed force, as shown in Fig. 10.

The third test was conducted by closing the bleed port so that the flow paths were through the piston orifices and shim stacks. The values of the stiffness, K_{spring}, and preload force, $F_{preload}$, were identified by fitting from tests with different frequencies. Figs. 12 and 13 show the results for the excitation frequency for different frequencies and amplitudes. It can be seen from the figures that the shim-stack dynamics greatly affect the characteristics of the damper due to the nonlinear characteristics of the shim stacks.

With confidence in the identified parameters for the bleed port, piston orifices, and shim stacks, overall validation was explored without the field-dependent damping force of the MR device. The identified parameter values of the model are listed in Table 3. Figs. 14 and 15 show the force vs. velocity curves for different frequencies and amplitudes. It can be observed that the model produces force vs. velocity plots with relatively good agreement with respect to the magnitude of the force and the nonlinear trend of the forces. One reason the model does not precisely match the experimental data is the absence of fluid compressibility in the model, which can cause

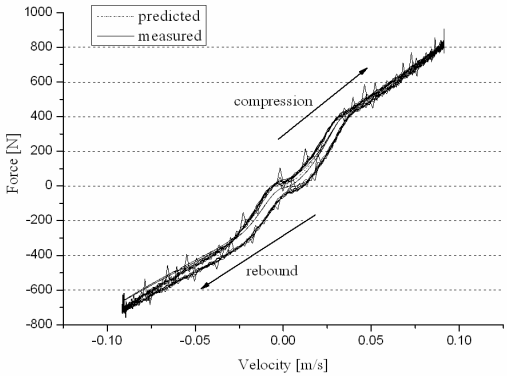

Fig. 13. Comparison between the predicted results and measured data for an oscillation frequency of 3.0 Hz with a 20 mm-displacement amplitude in the absence of an applied magnetic field.

hysteresis, and the absence of a force due to the momentum change of the fluid. Also, leakage flow is not included in this model. Leakage flow may lessen the damping force with prolonged usage. The shim stacks in the damper test exhibit highly nonlinear characteristics that cause a gradual decrease in the force vs. velocity gradient at higher velocities. This point was beyond the scope of this work and will be taken into account in future study.

The goal of this work has been to obtain a variable damper force by means of control of the applied current in an MR device. Figs. 16 and 17 describe the major characteristics of the hybrid damper that invokes the field-dependent damping force of the MR device. The measured damping-force characteristics obtained by gradually increasing the current from 0 to 0.8 amperes are shown in Figs. 16 and 17. As the applied magnetic field increases, the damping force also increases due to the increasing resistive force. In Fig. 16, a gain of nearly 37% is observed when the current is increased from 0A to 0.8A, i.e., an increase in the compression peak value from about 1012N to 1381N and a decrease in the rebound stroke peak from about -896N to -1237N. For an excitation frequency of 3Hz, the hysteresis loop widens and the hysteresis slope decreases, as shown in Fig. 17. The peak forces at 0A

Table 3. Identified parameter values of the model.

Compression parameters	
K_{bleed}	195 $[kg/mm^{(0.5)}m^{(0.75)}]$
K_{hys}	0.8 $[kg]$
$K_{orifice}$	1500 $[kg/mm^{(0.5)}m^{(0.75)}]$
$F_{preload}$	215 [N]
K_{spring}	72 $[kg/s]$
Rebound parameters	
K_{bleed}	150 $[kg/mm^{(0.5)}m^{(0.75)}]$
K_{hys}	4.5 $[kg]$
$K_{orifice}$	6300 $[kg/mm^{(0.5)}m^{(0.75)}]$
$F_{preload}$	400 [N]
K_{spring}	810 $[kg/s]$

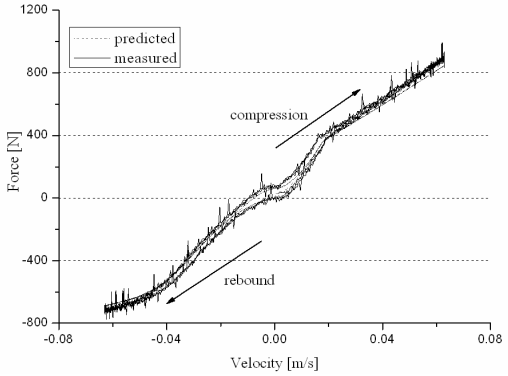

Fig. 14. The force vs. velocity curve of the hybrid damper for a piston-orifice correlation in the absence of an applied magnetic field with an excitation frequency of 1 Hz and a magnitude of 0.02 m.

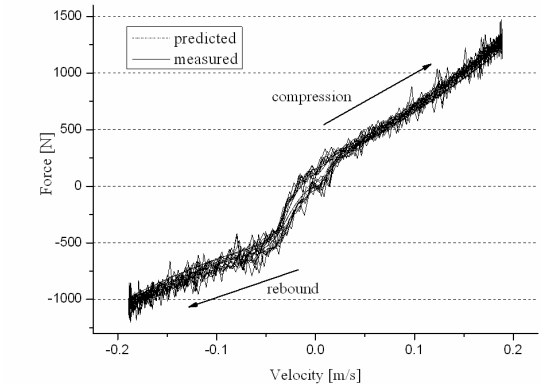

Fig. 15. The force vs. velocity curve of the hybrid damper for a piston-orifice correlation in the absence of an applied magnetic field with an excitation frequency of 3 Hz and a magnitude of 0.02 m.

and 0.8A are 1217N and 1744N, respectively, in compression and -1005N and -1482N, respectively, in rebound. The Bingham-like behavior, which consists of the field-dependent yield force, and the viscous damping force are clearly seen in the low- and high-velocity regions, respectively. The behavior of the viscous damping force corresponds to that of a force that is generated by an oil damper, while the behavior of the field-dependent yield force corresponds to that of the damping force of an MR device. In the near zero-velocity region, the characteristic hysteresis loop is mainly due to the frictional forces of the seal components inside the damper and especially the MR device. In reality, the MR device can only provide a force in the direction opposite to that of the relative velocity and undergoes a bleed of fluid between the bobbin and flux return part in the direction change of device, which results in a discrepancy between the force curves at small velocities. This frictional force also behaves as the field-dependent yield force. When a magnetic field is applied to the MR device, the sum of the field-dependent yield force and the frictional force affects the hysteresis behavior of the MR device. From the experimental investigation of the hybrid damper, it has been shown that the hybrid damper exhibits a very broad variation of the damping force under a magnetic field.

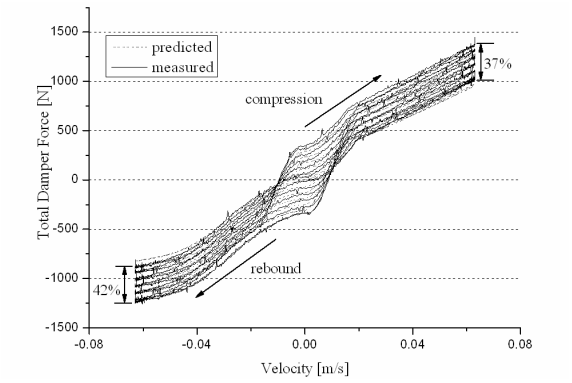

Fig. 16. The force vs. velocity curve of the hybrid damper for a piston-orifice correlation in the presence of an applied magnetic field with an excitation frequency of 1 Hz and a magnitude of 0.02 m.

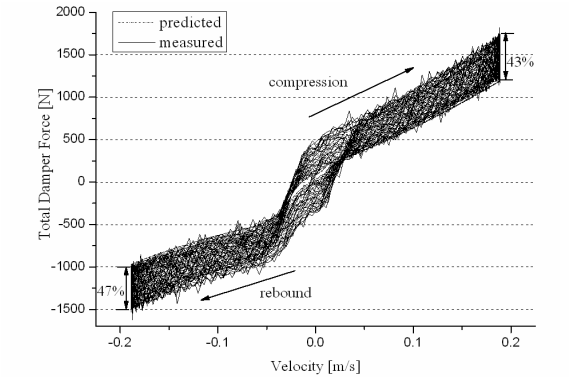

Fig. 17. The force vs. velocity curve of the hybrid damper for a piston-orifice correlation in the presence of an applied magnetic field with an excitation frequency of 3 Hz and a magnitude of 0.02 m.

5. Conclusions

This paper presented the development, modeling, and testing of a hybrid, semi-active damper, which can be applicable to a vehicle suspension. A mathematical model of a conventional passive oil damper was constructed and developed in

Matlab/Simulink, using the algorithm proposed by Reybrouck. Also, the characteristics of the MR device, which was used to resist the movement of the floating piston, were investigated; the Bouc-Wen model was adopted for the mathematical model. The parameters were identified by fitting the measured data with the predicted results. To achieve good results, several iterative processes were accomplished. It has been shown that the hybrid damper exhibits a broad variation with regard to the damping force in relation to the applied current in the MR device. It is also observed that for the performance of a conventional oil damper, an improvement of nearly 35% can be achieved by using different current levels. According to the results, this idea is feasible for characterizing the performance of semi-active dampers. The results presented in this work are still preliminary for the development of hybrid dampers. More research work will be undertaken for practical applications in the near future.

References

[1] D. Karnopp, M. J. Crosby and R. A. Harwood, Vibration control using semi-active force generators, *ASME J. Eng. Ind.*, 96 (2) (1974) 619-626.

[2] K. Yi and B. S. Song, A new adaptive sky-hook control of vehicle semi-active suspensions, *Proc. of the I MECH E Part D J. Automob. Eng.* 213 (3) (1999) 293-303.

[3] C. de Korh, Development of a new continuously variable damper for semi-active suspensions, *I. Mech. E. publication*, (C389/471) (1992) 141-151.

[4] S. H. Lee, J. H. Park, S. K. Lee, K. J. Youn and K. W. Min, Performance evaluation of passive and semi-active magnetorheological dampers, *J. of Mechanical Science and Technology*, 21 (6) (2007) 913-918.

[5] S. R. Hong, S. B. Choi, Y. T. Choi and N. M. Wereley, A hydro-mechanical model for hysteretic damping force prediction of ER damper: experimental verification, *J. of Sound and Vibration*, 285 (2005) 1180-1188.

[6] C. T. Lee and B. Y. Moon, Study on the damping performance characteristics analysis of shock absorber of vehicle by considering fluid force, *J. of Mechanical Science and Technology*, 19 (2) (2005) 520-528.

[7] K. Reybrouck, A nonlinear parametric model of an automotive shock absorber, *SAE 940869* (1994) 79-86.

[8] A. Sorniotti, N. D'Alfrio and A. Morgando, Shock absorber modeling and experimental testing, *SAE 2007-01-0855*, 2007.

[9] J. M. Gere and S. Timoshenko, Mechanics of Materials, Third Ed. International Thomson Publishing, pp 488-490.

[10] M. Ahmadian and J. A. Norris, Experimental analysis of magnetorheological dampers when subjected to impact and shock loading, *Communication in Nonlinear Science and Numerical Simulation*, 13 (9) (2008) 1983-1984.

[11] B. F. Spencer Jr, S. J. Dyke, M. K. Sain and J. D. Carlson, Phenomenological model for magnetorheological dampers, *J. of Eng. Mech.*, 123 (3) (1997) 230-238.

Young-Won Yun was born in Busan, Korea, in 1973. He received his B.S. in Mechanical Engineering from Dong-a University, Busan, Korea, in 2000. He also received his M.S. in Mechanical Engineering from Pusan National University, Busan, Korea, in 2003. He is currently working toward his Ph. D at Pusan National University. His current research interests are Electro-hydraulic systems and a robust controller.

Seong-Min Lee received the B.S. degree in Mechanical Engineering from Dong-a University in 2002. He also received his M.S. degree in Interdisciplinary programs in Mechatronics from Pusan National University in 2004, and now is a Ph.D. Candidate in Interdisciplinary in Mechatronics at Pusan National University in Korea. His research field is hydraulic control systems, hydraulic component design and energy saving in hydraulic systems.

Myeong-Kwan Park received the M.S. and Ph.D. degrees from Tokyo Institute of Technology, Tokyo, Japan, in 1988 and 1991, respectively, in mechanical engineering. From 1991 to 1992, he served as a Research Associate in Department Mechanical Engineering, Tokyo Institute of Technology. He is currently a full professor with Department of Mechanical Engineering and a Researcher in the Research Institute of Mechanical Technology at Pusan National University. His research interests are in hydraulic and smart fluid such as magnetic fluid, ER fluid and MR fluid.